



Deposited via The University of Sheffield.

White Rose Research Online URL for this paper:

<https://eprints.whiterose.ac.uk/id/eprint/205826/>

Version: Published Version

Article:

Huang, W., Zeng, J., Jia, L. et al. (2023) Genetic risks of Alzheimer's by APOE and MAPT on cortical morphology in young healthy adults. *Brain Communications*, 5 (5). ARTN fcad234. ISSN: 2632-1297

<https://doi.org/10.1093/braincomms/fcad234>

Reuse

This article is distributed under the terms of the Creative Commons Attribution (CC BY) licence. This licence allows you to distribute, remix, tweak, and build upon the work, even commercially, as long as you credit the authors for the original work. More information and the full terms of the licence here:

<https://creativecommons.org/licenses/>

Takedown

If you consider content in White Rose Research Online to be in breach of UK law, please notify us by emailing eprints@whiterose.ac.uk including the URL of the record and the reason for the withdrawal request.

BRAIN COMMUNICATIONS

Genetic risks of Alzheimer's by *APOE* and *MAPT* on cortical morphology in young healthy adults

Weijie Huang,^{1,2,3,*} Jianmin Zeng,^{4,*} Lina Jia,⁵ Dajiang Zhu,⁶  John O'Brien,⁷ Craig Ritchie,^{8,9} Ni Shu¹ and Li Su^{2,7}

* These authors contributed equally to this work.

Genetic risk factors such as *APOE* $\epsilon 4$ and *MAPT* (rs242557) A allele are associated with amyloid and tau pathways and grey matter changes at both early and established stages of Alzheimer's disease, but their effects on cortical morphology in young healthy adults remain unclear. A total of 144 participants aged from 18 to 24 underwent 3T MRI and genotyping for *APOE* and *MAPT* to investigate unique impacts of these genetic risk factors in a cohort without significant comorbid conditions such as metabolic and cardiovascular diseases. We segmented the cerebral cortex into 68 regions and calculated the cortical area, thickness, curvature and folding index for each region. Then, we trained machine learning models to classify *APOE* and *MAPT* genotypes using these morphological features. In addition, we applied a growing hierarchical self-organizing maps algorithm, which clustered the 68 regions into 4 subgroups representing different morphological patterns. Then, we performed general linear model analyses to estimate the interaction between *APOE* and *MAPT* on cortical patterns. We found that the classifiers using all cortical features could accurately classify individuals carrying genetic risks of dementia outperforming each individual feature alone. *APOE* $\epsilon 4$ carriers had a more convoluted and thinner cortex across the cerebral cortex. A similar pattern was found in *MAPT* A allele carriers only in the regions that are vulnerable for early tau pathology. With the clustering analysis, we found a synergetic effect between *APOE* $\epsilon 4$ and *MAPT* A allele, i.e. carriers of both risk factors showed the most deviation of cortical pattern from the typical pattern of that cluster. Genetic risk factors of dementia by *APOE* $\epsilon 4$ and *MAPT* (rs242557) A allele were associated with variations of cortical morphology, which can be observed in young healthy adults more than 30 years before Alzheimer's pathology is likely to occur and 50 years before dementia symptoms may begin.

- 1 State Key Laboratory of Cognitive Neuroscience and Learning, Beijing Normal University, Beijing 100875, China
- 2 Department of Neuroscience, Neuroscience Institute, Insigneo Institute for In Silico Medicine, University of Sheffield, Sheffield S10 2HQ, UK
- 3 School of Systems Science, Beijing Normal University, Beijing 100875, China
- 4 Faculty of Psychology, Sino-Britain Centre for Cognition and Ageing Research, Southwest University, Chongqing 400715, China
- 5 Beijing Anding Hospital, Capital Medical University, Beijing 100088, China
- 6 Department of Computer Science and Engineering, University of Texas at Arlington, Arlington, TX 76019, USA
- 7 Department of Psychiatry, School of Clinical Medicine, University of Cambridge, Cambridge CB2 0SZ, UK
- 8 Edinburgh Dementia Prevention and Centre for Clinical Brain Sciences, Edinburgh Medical School, University of Edinburgh, Edinburgh EH4 2XU, UK
- 9 Scottish Brain Sciences, Edinburgh EH12 9DQ, UK

Correspondence to: Li Su, PhD,
Department of Neuroscience, Sheffield Institute for Translational Neuroscience
University of Sheffield, 385a Glossop Road
Sheffield S10 2HQ, South Yorkshire, UK
E-mail: l.su@sheffield.ac.uk

Received March 10, 2023. Revised July 29, 2023. Accepted August 30, 2023. Advance access publication September 8, 2023

© The Author(s) 2023. Published by Oxford University Press on behalf of the Guarantors of Brain.

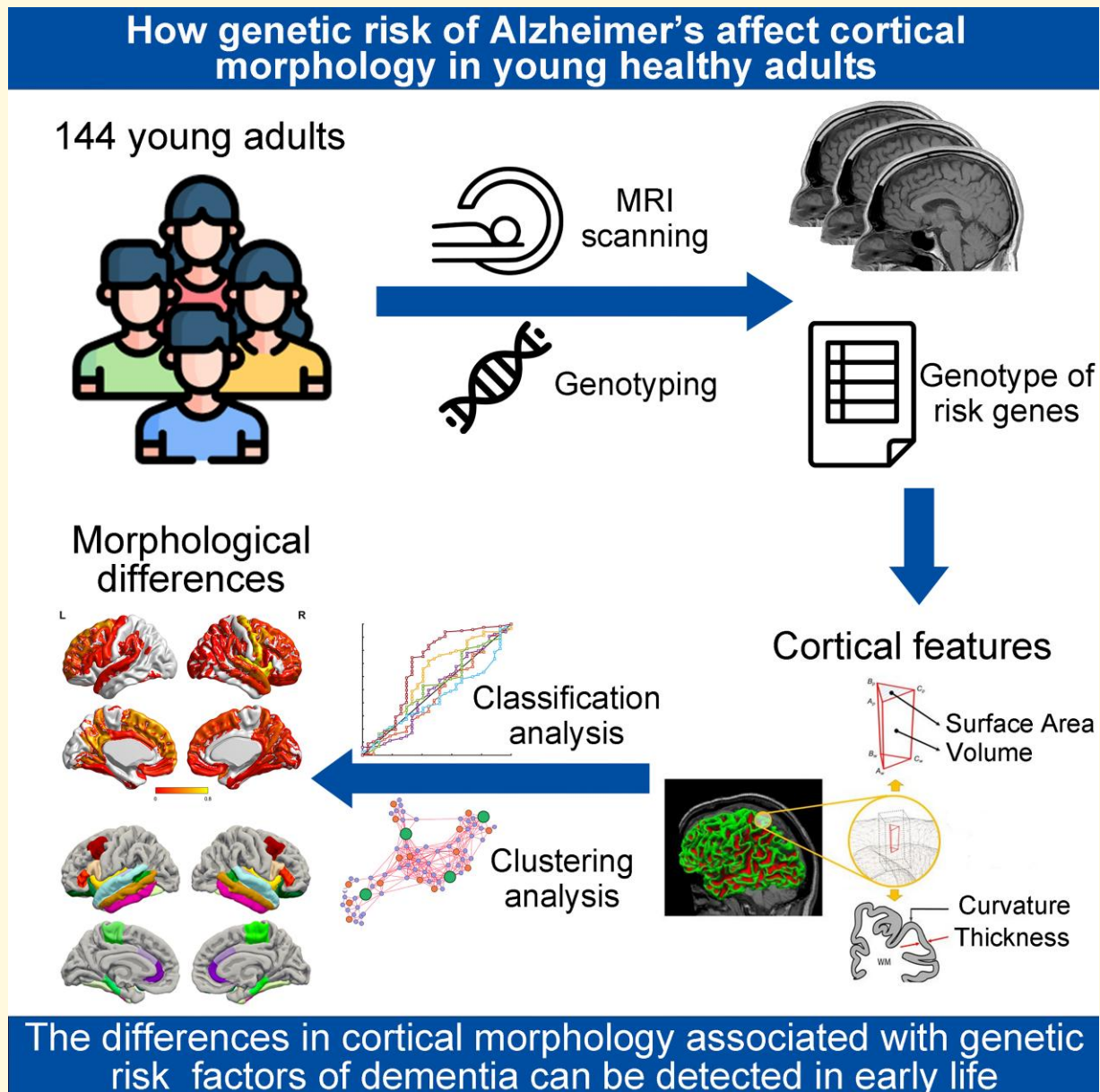
This is an Open Access article distributed under the terms of the Creative Commons Attribution License (<https://creativecommons.org/licenses/by/4.0/>), which permits unrestricted reuse, distribution, and reproduction in any medium, provided the original work is properly cited.

Correspondence may also be addressed to: Jianmin Zeng, PhD,
Faculty of Psychology, Sino-Britain Centre for Cognition and Ageing Research
Southwest University, No. 2, Tiansheng Road, Chongqing, Chongqing 400715, China
E-mail: james_psych@yeah.net

Correspondence may also be addressed to: Ni Shu, PhD,
State Key Laboratory of Cognitive Neuroscience and Learning
Beijing Normal University, No. 19, Xijiekouwai Street Beijing, Beijing 100875, China
E-mail: nshu@bnu.edu.cn

Keywords: genetic risk factor; machine learning; MRI; cortical thickness; cortical curvature

Graphical Abstract



Introduction

The 2018 Amyloid, Tau and Neurodegeneration (ATN) research framework for Alzheimer's disease (AD) provides a systematic method to determine AD continuum designation.¹ In this framework, extracellular amyloid beta ($A\beta$) plaques and intracellular hyperphosphorylated tau neurofibrillary tangles are the two most important pathological hallmarks, which precede neurodegeneration. As the most common genetic risk, apolipoprotein E (*APOE*) $\epsilon 4$ relates to impaired $A\beta$ clearance,^{2,3} thus increasing the formation of plaques leading to AD. Microtubule-associated protein tau (*MAPT*) rs242557 with the major allele G and the minor allele A is also related to tauopathies via differential expression of various exons relevant to tau aggregation.⁴⁻⁶ *MAPT* rs242557 (*MAPT* for short) has been associated with increased risk of AD, and there is emerging evidence for an additive effect of *APOE* and *MAPT* in modulating the risk for AD.⁷

APOE $\epsilon 4$ not only participates during pathological processes in patients with AD but also impairs cortical structure in non-demented older individuals. For instance, previous studies found that for individuals with subjective cognition decline, *APOE* $\epsilon 4$ carriers showed reduced volume in the left hippocampus^{8,9} and reduced cortical area in the right hemisphere^{8,10} than non-carriers. To the best of our knowledge, there is no existing data about the specific influence of *MAPT* on cerebral structure, but a previous study reported that patients with mild cognitive impairment (MCI) carrying *MAPT* haplotype H1 showed an increased volume in bilateral superior frontal gyri and precentral gyrus as well as in left inferior temporal gyrus and calcarine gyrus.¹¹ However, the precise effects of *MAPT* on brain structure and how it interacts with *APOE* $\epsilon 4$ remain unclear.

In addition, a cross-lifespan study showed that genes have a lifelong impact on the trajectory of development and aging of the cortical cortex, in which individuals' cortical thickness decreased rapidly in the first 20 years of life and after the age of 50 years old but kept relatively stable between 20 and 50 years of age.¹² Brain areas which showed the most changes before the age of 20 also mirror the areas which showed the fastest decline after the age of 50.¹² Hence, early 20s is an important time point in life to investigate the early genetic effect on the development of the human cerebral cortex and how genetic predisposition may have a lifelong impact on the brain. However, the existing literature on the effect of *APOE* $\epsilon 4$ on cerebral structure in young adults remains inconsistent. Some studies found that *APOE* $\epsilon 4$ has detrimental effects on hippocampal volume¹³ and entorhinal thickness,¹⁴ but others found no statistically significant difference between *APOE* $\epsilon 4$ carriers and non-carriers at this stage.¹⁵⁻¹⁷ Due to the absence of previous research investigating the relationship between *MAPT* and cerebral structure in young adults, its influence in early life remains unclear. The mixed findings may be attributed to the small sample size in previous studies and the fact that the effect of *APOE* in young adults is too subtle to be detected using conventional univariate analyses. Recent studies highlighted the benefits of

multivariable approaches compared with univariate methods when assessing the differences in hippocampal volume between *APOE* $\epsilon 4$ and non-carriers.¹⁸ In addition, most previous studies only focused on thickness and volume of the cerebral cortex but neglected other measures of cortical folding patterns such as curvature and folding index, which have been demonstrated to be sensitive to AD pathology.¹⁹ Finally, most previous studies also suffer from relatively small sample sizes thus the lack of adequate statistical power to detect reliable effects.

Hence, the aim of this study was to use multivariable methods incorporating additional cortical folding information in a large cohort to examine the impacts of *APOE* $\epsilon 4$ and *MAPT* A allele on healthy young adults. We expect ultra-early structural differences to occur in medial prefrontal and temporal lobes, cingulum, precuneus cortex and hippocampus, because these brain regions are known to be vulnerable for early Alzheimer's pathology.

Materials and methods

Participants

A total of 155 self-declared Han Chinese college students aged 18–24 were recruited from Southwest University using advertisements. We have focused on Han population because previous studies showed that the *APOE* $\epsilon 4$ allele is significantly more prevalent in Han than non-Han ethnic Chinese, making Han Chinese at higher risk of developing dementia.²⁰⁻²² All participants provided written informed consent. This study was approved by the Ethic Committee of Psychological Research at Southwest University, Chongqing City, China. Of the 155 participants, 11 were excluded from the MRI analysis because of excessive head motion.

Image acquisition and processing

Whole-brain T_1 -weighted scan [MPRAGE, 160 slices, voxel size 1.0 mm,³ repetition time (TR) = 2300 ms, echo time (TE) = 2.98 ms, flip angle (FA) = 9°] was acquired using a Siemens Verio 3T MRI scanner. Structural MRI images were processed using FreeSurfer v5.3 (<http://surfer.nmr.mgh.harvard.edu/>) to calculate cortical area, thickness, curvature, folding index and subcortical volume. Specifically, imaging processing included motion correction and averaging²³ of multiple volumetric T_1 -weighted images (when more than one is available), removal of non-brain tissue using a hybrid watershed/surface deformation procedure,²⁴ automated Talairach transformation, segmentation of the subcortical white matter and deep grey matter volumetric structures (including hippocampus, amygdala, caudate, putamen and ventricles)^{25,26} intensity normalization,²⁷ tessellation of the grey/white matter boundary, automated topology correction^{28,29} and surface deformation following intensity gradients to optimally place the grey/white and grey/cerebrospinal fluid borders at the location where the greatest shift in intensity defines the transition to the other tissue class.³⁰⁻³²

Then, the whole-brain MRI images were parcellated into 34 regions per hemisphere according to the Desikan–Killiany Atlas.³³ Surface area was measured at the grey/white matter boundary, and thickness was measured as the average distances in a region between the white matter and pial surfaces. At each vertex, FreeSurfer measured the mean curvature as follows:

$$H = (K_1 + K_2)/2,$$

and the folding index as follows:

$$FI = |K_1| \times (|K_1| - |K_2|),$$

where K_1 and K_2 denote the maximum and minimum normal curvature.³⁴ Then, the regional mean curvature and folding index were calculated.

Multivariate discriminative analysis

To construct models that can identify individuals carrying increased genetic risks for AD, we trained support vector machine (SVM) models and evaluated their performance with 5-fold cross-validation which is a standard method used in machine learning to avoid over-fitting. The pipeline consisted of the following three steps: (i) feature extraction and selection, (ii) model training and evaluation and (iii) identifying the most discriminative features, which we will explain in turn. The below pipeline was performed for classifying *APOE* $\epsilon 4$ positive (*APOE+*) individuals from negative (*APOE-*) individuals and rs242557 A positive (*MAPT+*) individuals from negative (*MAPT-*) individuals, respectively.

Feature extraction and selection

For each participant, we extracted cortical area, mean thickness, mean curvature and mean folding index from 68 regions defined by Desikan–Killiany Atlas and volume of the 14 subcortical nuclei as features for SVM. We did not include cortical volume because it is redundant considering that cortical area and mean thickness are included as features. We separated the data set into training and test data set to perform 5-fold cross-validation, and the specific approach to split data is described in the next section. In each fold, we performed generalized linear model (GLM) analyses to compare the differences in all the features between two groups in the training data set while controlling for age, sex and education. For both training and test data sets, only those features with P -value < 0.05 were kept. Then, we normalized the features with the mean and standard deviations of the corresponding features from the training data set.

Model training and evaluation

As we mentioned before, a standard machine learning method with 5-fold cross-validation was used to evaluate the model's performance. Specifically, we randomly divided the data set into five subsets that have almost the same proportion of participants with higher genetic risk as that of the whole data set with stratified random sampling. In each fold, we used

four subsets as training data set and the remaining subset as the test data set. The training data set was used to train a linear SVM model with the soft margin parameter $C = 1$, and the test data set was then used to evaluate the performance of the trained model. When the 5-fold cross-validation finished, we obtained predicated labels of all participants. The most common measures, accuracy, sensitivity, specificity and the area under curve, were used to evaluate model performance. In addition, we also used positive predictive value and negative predictive value, which depends on not only the model itself but also the prevalence and F -score to estimate the models' performance because these metrics are more reliable in interpreting the classification results from an unbalanced data set. All values are defined as follows:

$$\text{Accuracy} = \frac{TP + TN}{TP + FN + TN + FP}$$

$$\text{Sensitivity} = \frac{TP}{TP + FN}$$

$$\text{Specificity} = \frac{TN}{TN + FP}$$

$$\text{PPV} = \frac{TP}{TP + FP}$$

$$\text{NPV} = \frac{TN}{TN + FN}$$

$$F = 2 \times \frac{\text{PPV} \times \text{sensitivity}}{\text{PPV} + \text{sensitivity}},$$

where TP, FN, TN, FP, PPV, NPV and F denote the number of positive instances correctly predicted (hit), the number of positive instances classified as negative instances (miss), the number of negative instances correctly predicted (correct rejection), the number of negative instances classified as positive instances (false alarm), positive predictive value, negative predictive value and F -score, respectively. We then tested each index statistically using permutation testing, which indicates whether the observed index is significantly different from that of random models. Specifically, we re-applied the classification procedure 1000 times. In each run, we permuted all the labels across the samples without replacement. The significance was determined by ranking the above-observed indexes in the null distribution; the P -value of each index was the proportion of permutations that showed a higher value than the observed true value.

Identifying the most discriminative features

The training of SVM model is based on the determination of the separating hyperplane, which is orthogonal to the discrimination hyperplane or projective direction. It has been shown that the coefficients of the discrimination hyperplane quantify the amount of discriminative feature information.^{35,36} To determine which brain region contributed the most to the prediction, we summed the absolute values of coefficients of all cortical metrics of each region. The absolute values were used to quantify the regions' contribution to the classification. Similarly, to determine which cortical

metrics contributed to the classification, we summed the coefficients of all regions positively related to the outcome and the regions negatively related to the outcome separately.

Morphological clustering analysis

To investigate the gene–gene interaction between *APOE* and *MAPT* on the imaging features, we used clustering model rather than classification that is unsuitable to evaluate interaction effect. To cluster the regions, we trained a growing hierarchical self-organizing maps (GHSOM) model, which is an artificial neural network and provides a means of representing multidimensional data set as a 2D map.³⁷ The features we used here was the same as those in discriminative analysis, and their Z-scores were input into model for training. Once trained, this map is a model of the original input data, with individual measures represented as individual weight planes (or layers). Each node corresponds to a weight vector with the same dimensionality as the input data. The nodes in the top layer can be regarded as the centroids of the clusters, i.e. the typical pattern of the class. Then, we assigned every region to the cluster that has the closest distance from the centroids/region. For each participant and each cluster, the intra-cluster distance was calculated by averaging distances from regions to the cluster centroid.

Statistical analysis

Group comparisons of demographics were performed with analysis of variance and chi-square test. GLM analyses were used to statistically explore the effect of *APOE* and *MAPT* on cortical morphology characteristics including thickness, area, volume, mean curvature and folding index and subcortical volume controlling for age, sex and education. When comparing volume between groups with different genotypes, total intracranial volume was also controlled for. False discovery rate was used to correct for multiple comparisons in the demographics analysis and univariate analysis.

We used GLM analyses to statistically test for the effects of *APOE*, *MAPT* and their interactions on the four

intra-cluster distances controlling for age, sex and years of education. Bonferroni correction was used to correct for multiple comparisons in the clustering analysis. For the cluster showing a significant interaction effect on the intra-cluster distance among groups, we also compared the mean cortical metrics from all regions belonging to that cluster. Threshold for statistical significance was set at $P < 0.05$, two-sided in all analyses.

Results

Demographic characteristics of the samples

The samples consisted of 83 individuals without neither genetic risk factor studied here, 11 individuals only carrying *APOE* $\epsilon 4$, 34 individuals with genetic risk due to the *MAPT* locus alone and 16 individuals with both genetic risks. Their age ($P = 0.784$), sex ($P = 0.393$) and education ($P = 0.536$) were not statistically different between groups. Detailed descriptions and the demographics of the samples are provided in Table 1.

Group differences in cerebral structure using univariate analysis

We compared cortical thickness, area, volume, mean curvature and folding index and subcortical volume between *APOE* $\epsilon 4$ carriers and non-carriers using univariate tests. Similarly, we also compared these individual structural characteristics between *MAPT* A carriers and non-carriers. However, no result survived false discovery rate correction.

Classification between *APOE* $\epsilon 4$ carriers and non-carriers

We used 5-fold cross-validation to estimate the generalizability of the classifier between *APOE* $\epsilon 4$ carriers and non-carriers. As shown in Table 2, the classifier achieved a

Table 1 Demographics of all participants

	APOE–		APOE+		T/χ^2 (P)
Gender (M/F)	48/69		11/16		0 (0.978) ^a
Age; yr	18.5–23.9 (20.6 ± 0.9)		19.4–23.4 (20.6 ± 1.0)		0.39 (0.696) ^b
Years of education; yr	12–14 (12.4 ± 0.6)		12–14 (12.3 ± 0.5)		1.21 (0.229) ^b
	MAPT–		MAPT+		T/χ^2 (P)
Gender (M/F)	34/60		25/25		2.58 (0.108) ^a
Age; yr	18.5–23.9 (20.6 ± 0.9)		18.7–23.4 (20.6 ± 0.9)		0.10 (0.921) ^b
Years of education; yr	12–14 (12.4 ± 0.6)		12–14 (12.3 ± 0.6)		0.55 (0.582) ^b
	APOE–MAPT–		APOE+MAPT–		F/χ^2 (P)
Gender (M/F)	31/52	3/8	17/17	8/8	2.99 (0.393) ^a
Age; yr	18.5–23.9 (20.6 ± 0.9)	19.5–22.3 (20.4 ± 0.8)	18.7–22.3 (20.6 ± 0.8)	19.4–23.4 (20.7 ± 1.1)	1.07 (0.784) ^c
Years of education; yr	12–14 (12.4 ± 0.6)	12–13 (12.2 ± 0.4)	12–14 (12.4 ± 0.5)	12–14 (12.3 ± 0.6)	2.18 (0.536) ^c

APOE–, *APOE* $\epsilon 4$ non-carriers; APOE+, *APOE* $\epsilon 4$ carriers; MAPT–, MAPT rs242557 A non-carriers; MAPT+, MAPT rs242557 A carriers.

^a T/χ^2 (P) value for comparison with a chi-square test.

^b T/χ^2 (P) value for comparison with a two-sample t-test.

^c F/χ^2 (P) value for comparison with an analysis of variance.

Table 2 Classification performances

APOE ϵ4 non-carriers versus APOE ϵ4 carriers						
	All features	Cortical area	Cortical thickness	Cortical curvature	Cortical folding index	Subcortical volume
Accuracy	0.81 (0.028)	0.79 (0.086)	0.79 (0.086)	0.81 (0.028)	0.78 (0.217)	0.81 (0.028)
Sensitivity	0.52 (0.001)	0 (1)	0 (1)	0 (1)	0.07 (0.35)	0 (1)
Specificity	0.88 (0.815)	0.98 (0.038)	0.98 (0.038)	1 (0.001)	0.95 (0.265)	1 (0.001)
Area under curve	0.66 (0.016)	0.47 (0.575)	0.61 (0.073)	0.49 (0.435)	0.52 (0.287)	0.44 (0.721)
Positive predictive value	0.5 (0.011)	0 (1)	0 (1)	0 (1)	0.25 (0.216)	0 (1)
Negative predictive value	0.89 (0.001)	0.81 (0.506)	0.81 (0.506)	0.81 (0.381)	0.82 (0.272)	0.81 (0.381)
F-score	0.51 (0.001)	0 (1)	0 (1)	0 (1)	0.11 (0.376)	0 (1)
MAPT rs242557 A non-carriers versus MAPT rs242557 A carriers						
	All features	Cortical area	Cortical thickness	Cortical curvature	Cortical folding index	Subcortical volume
Accuracy	0.63 (0.082)	0.65 (0.013)	0.62 (0.114)	0.63 (0.082)	0.65 (0.013)	0.65 (0.013)
Sensitivity	0.46 (0.013)	0 (1)	0.12 (0.854)	0.06 (0.964)	0.06 (0.964)	0 (1)
Specificity	0.71 (0.736)	1 (0.001)	0.83 (0.019)	0.93 (0.005)	0.97 (0.001)	1 (0.001)
Area under curve	0.61 (0.044)	0.55 (0.168)	0.58 (0.081)	0.48 (0.52)	0.56 (0.152)	0.51 (0.324)
Positive predictive value	0.47 (0.054)	0 (1)	0.35 (0.402)	0.30 (0.617)	0.50 (0.013)	0 (1)
Negative predictive value	0.71 (0.022)	0.65 (0.434)	0.65 (0.423)	0.65 (0.476)	0.66 (0.339)	0.65 (0.343)
F-score	0.46 (0.020)	0 (1)	0.18 (0.423)	0.1 (0.963)	0.11 (0.958)	0 (1)

The bold values represent the best performance.

classification accuracy of 0.81, a sensitivity of 0.52, a specificity of 0.88 and an area under curve of 0.66. As we mentioned above, the model's accuracy was also assessed with positive predictive value, negative predictive value and *F*-score that are more robust for our unbalanced data set. These metrics (positive predictive value: 0.50, $P = 0.011$; negative predictive value: 0.89, $P = 0.001$; *F*-score: 0.51, $P = 0.001$) were statistically significantly higher than those of random models. We compared the performance of model using all cortical features and the models using only a single feature. As shown in Fig. 1A, the model using all the features outperformed all other models based on single cortical feature demonstrating the advantage of multivariate approach including multiple cortical features in a single analysis.

The cortical distribution of positive and negative weights is presented in Fig. 1B and C, respectively, and no subcortical volumes contributed to the classification. Overall, the left superior frontal cortex, left precuneus, left isthmus of cingulate, right precentral cortex, right insula and right caudal middle frontal cortex were the most discriminative regions (Fig. 1D). In addition, the thickness of most brain regions was negatively relative to the presence of *APOE* ϵ 4 and the folding index of most affected brain regions was positively relative to the presence of *APOE* ϵ 4 (Fig. 1E).

Classification between MAPT A carriers and non-carriers

Similarly, we used 5-fold cross-validation to estimate the generalizability of the classifier between *MAPT* A allele carriers and non-carriers. As shown in Table 2, the classifier achieved a classification accuracy of 0.63, a sensitivity of 0.46, a specificity of 0.71 and an area under curve of 0.61. The positive predictive value, a negative predictive value

and an *F*-score of the classifier were 0.47, 0.71 and 0.46, respectively. The last three metrics were more robust and were all statistically significantly higher than that of random models. We compared the performance of model using all features and the models using just a single feature. As shown in Fig. 2A, the model using all features also outperformed other models similar to our previous analysis.

The distribution of positive and negative weights is presented in Fig. 2B and C, respectively, and volume of bilateral hippocampus, bilateral amygdala and right caudate also contributed to the classification. Overall, the left middle temporal cortex, left pericalcarine, left lateral orbitofrontal cortex, rostral anterior cingulate cortex, right pars orbitalis and banks of the superior temporal sulcus were the most affected regions (Fig. 2D). In addition, the thickness of most brain regions was negatively relative to the presence of *MAPT* A allele and the folding index of most affected brain regions was positively relative to the presence of *MAPT* A allele (Fig. 2E).

APOE-MAPT interaction on cortical features

As shown in Fig. 3A, the four nodes in the top layer represent the centroids of four clusters: (i) the brain regions with medium area, large thickness and small curvature; (ii) the brain regions with large area, small thickness and small curvature; (iii) the brain regions with small area, large thickness and large curvature; and (iv) and the brain regions with medium area, small thickness and large curvature. For ease of comparison, the weight profiles of the top layer of nodes are also plotted in Fig. 3B. The spatial distribution of the four clusters across all brain regions is shown in Fig. 3C.

GLM analyses showed a significant interaction ($T = -2.600$, $P = 0.009$) between *APOE* and *MAPT* such

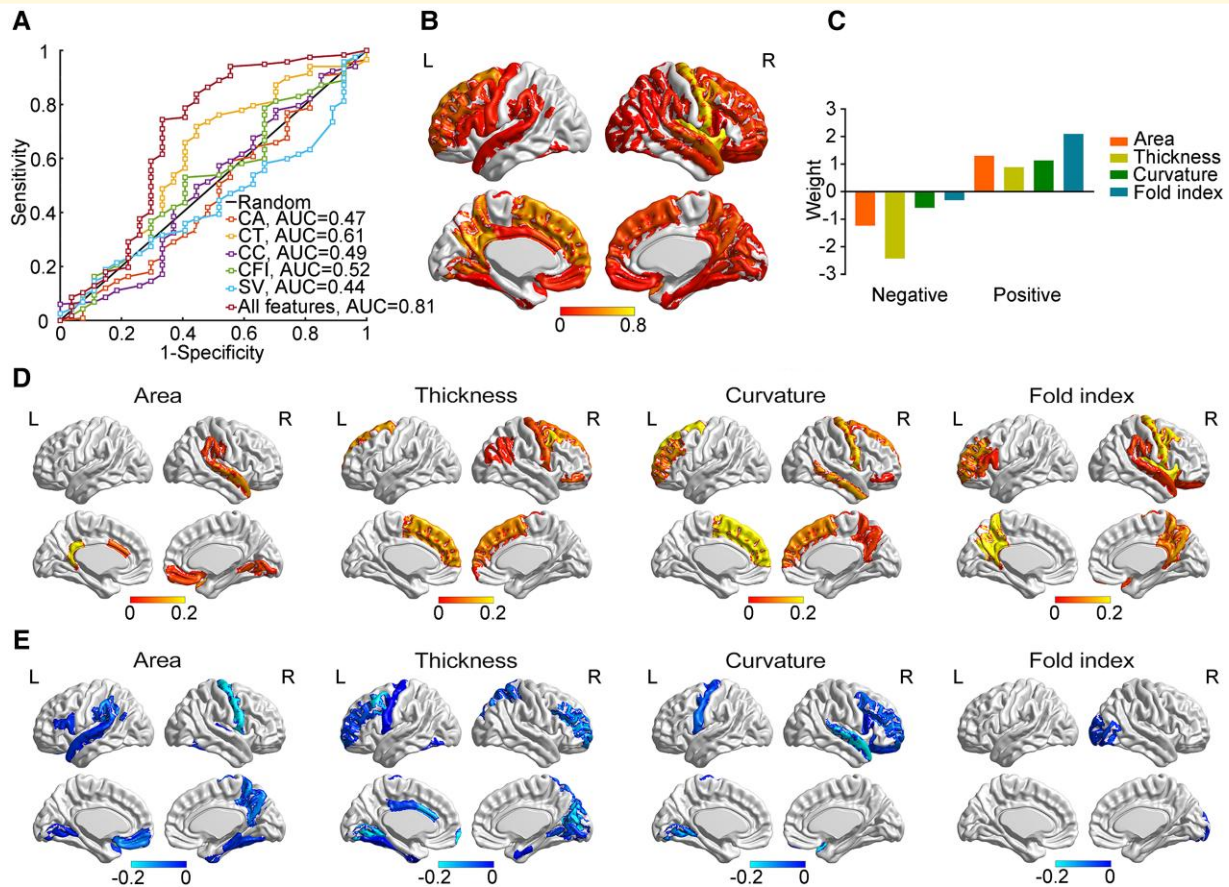


Figure 1 The classification between *APOE* $\epsilon 4$ carriers and non-carriers. **(A)** The receiver operating characteristic curve of the classification (*APOE* $\epsilon 4$ carriers, $n = 27$; *APOE* $\epsilon 4$ non-carriers, $n = 117$). **(B)** The map of positive weight. **(C)** The map of negative weight. **(D)** The sum of absolute weight across different measures. **(E)** The sum of weight across different regions. CA, cortical area; CT, cortical thickness; CC, cortical curvature; CFI, cortical fold index; SV, subcortical volume.

that individuals with both genetic risks had the significantly increased distance from the centroid of the first cluster comparing with the other groups (Fig. 4A). This deviation was mainly caused by the increase in curvature ($T = -2.379$, $P = 0.019$) and folding index ($T = -2.567$, $P = 0.011$) (Fig. 4B). While there was no difference in distance from the centroid in other three clusters, we also compared their mean cortical measurements. Similar gene–gene interaction on the folding index in regions from the second cluster ($T = -2.034$, $P = 0.044$) (Fig. 5B) and the curvature of the regions in the fourth cluster ($T = -2.258$, $P = 0.026$) (Fig. 5D) was found.

Discussion

The present study yielded a main finding that *APOE* $\epsilon 4$ and *MAPT* A allele had a synergetic effect on cerebral cortical morphology especially in a network of brain regions including the bilateral lateral and medial temporal cortex, anterior cingulate, paracentral cortex, insula, lateral orbitofrontal cortex, pars orbitalis and caudal middle frontal cortex as

early as early adulthood. The carriers with both risk genes showed a different cortical morphology, namely increasing curvature and folding index and decreased thickness in these regions.

Early effect of *APOE* on cortical morphology

The SVM model separating *APOE* status based on cerebral structural features showed a significant discriminability between *APOE* $\epsilon 4$ carriers and non-carriers, which indicated that young healthy adults carrying *APOE* $\epsilon 4$ had a different pattern of cerebral structure from non-carriers. By analysing the model's weights, the individuals carrying *APOE* $\epsilon 4$ have higher folding index and curvature and lower thickness across widespread regions of the cerebral cortex. Regarding the most discriminative regions, the right precentral cortex, right insula, left superior frontal cortex, right superior temporal cortex and right caudal middle frontal cortex were the top five regions that contributed most to the classification. This is consistent with previous studies showing that the superior temporal cortex¹¹ and insula³⁸

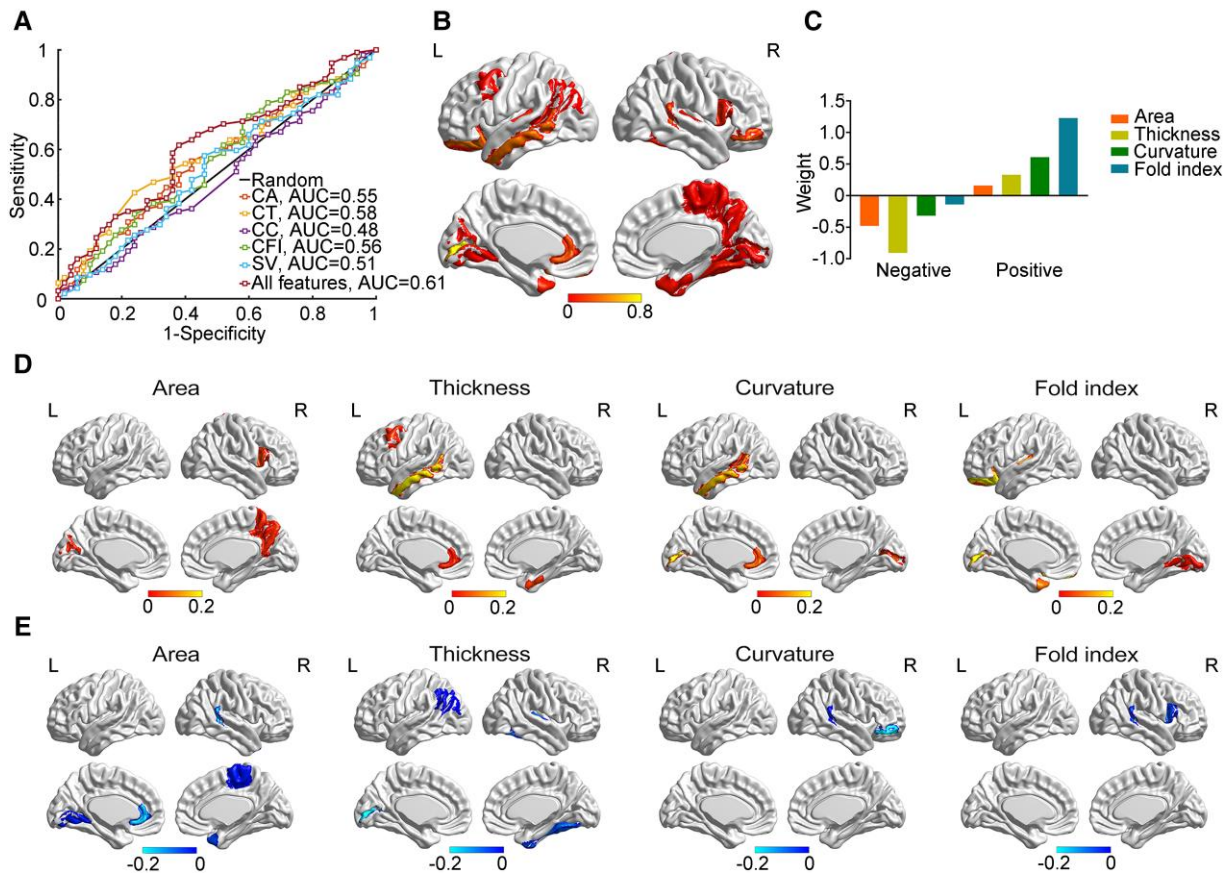


Figure 2 The classification between *MAPT* rs242557 A carriers and non-carriers. (A) The receiver operating characteristic curve of the classification (*MAPT* A carriers, $n = 50$; *MAPT* A non-carriers, $n = 94$). (B) The map of positive weight. (C) The map of negative weight. (D) The sum of absolute weight across different measures. (E) The sum of weight across different regions. CA, cortical area; CT, cortical thickness; CC, cortical curvature; CFI, cortical fold index; SV, subcortical volume.

have reduced grey matter volume in amnesic mild cognitive impairment with *APOE* $\epsilon 4$ compared with non-carriers. Furthermore, a longitudinal study showed that *APOE* $\epsilon 4$ accelerated brain atrophy in superior temporal gyrus in healthy older participants.³⁹ The right precentral cortex, left superior frontal cortex and right caudal middle frontal cortex showed thinner cortex or lower grey matter volume already in middle-aged healthy individuals with *APOE* $\epsilon 4$.^{40,41} Our results extend the existing knowledge about the relationship between *APOE* $\epsilon 4$ and altered cortical morphology from middle-aged and older people to young healthy adults, when AD pathology was unlikely.

Early effect of *MAPT* on cortical morphology

Although the model discriminating the *MAPT* status had a slightly lower performance than the model classifying the *APOE* status, it significantly outperformed random models in terms of the *F*-score test. Across the cerebral cortex, the model for *MAPT* showed a similar pattern as the *APOE* analysis, that is, individuals carrying *MAPT* A allele have higher

folding index and lower thickness. The difference between two models is that the number of regions contributing to classifying *MAPT* status is less than that for *APOE*. However, most of these regions identified in the SVM analysis were those implicated in the early phase of Braak pathological staging for tau and amyloid beta, such as the entorhinal cortex, fusiform, lingual, middle temporal, cingulate and temporal pole.⁴² Although we did not have biomarker evidence for tau and amyloid pathology in this study, it is reasonable to assume that our young healthy cohort was free from AD pathology as well as other comorbidities found in patients with established AD. So, the current findings might represent a pure genetically determined neuroanatomical trait which makes these individuals more vulnerable to AD pathology in the future.

Interaction between *APOE* and *MAPT* in early adulthood

The GHSOM clustering analysis showed that in our cohort, the cerebral cortex could be separated into four major morphologically distinct networks; each is composed of several

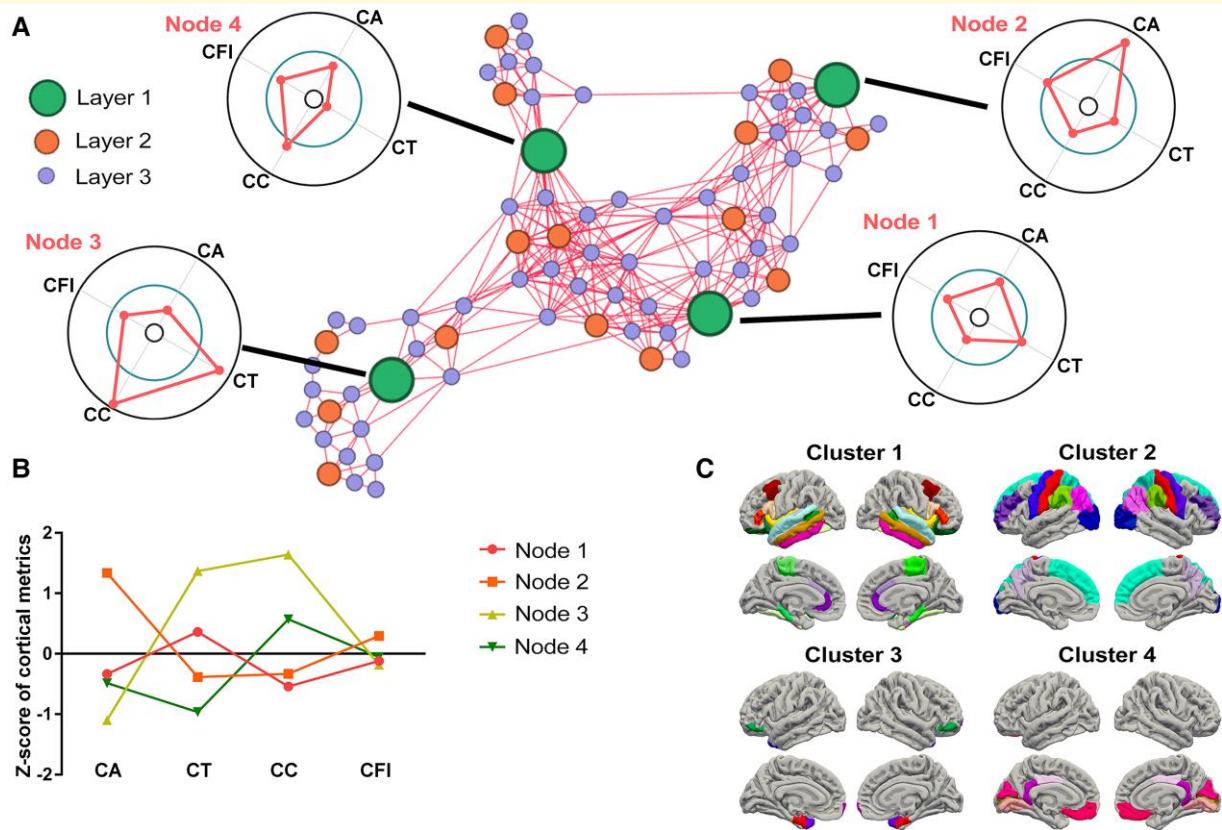


Figure 3 The cortical morphological profiles defined by neural network and their distributions. **(A)** Graphical representation of the top three-layer representation, using Euclidean distance and a Force Atlas layout in Gephi toolkit. The biggest nodes correspond to the top layer of nodes, which represent the final clusters, and the radar plots show the profiles of those nodes. **(B)** The profiles of the clusters overlaid. **(C)** The spatial distribution of clusters. CA, cortical area; CT, cortical thickness; CC, cortical curvature; CFI, cortical fold index.

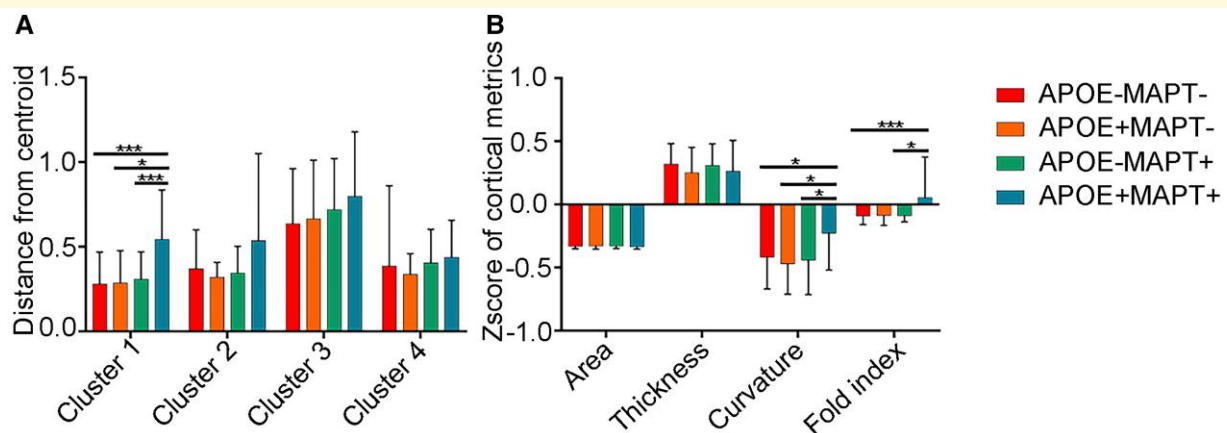


Figure 4 The interaction effect between *APOE* and *MAPT* rs242557 on cortical morphology. **(A)** The differences in distance from the centroid of cluster among four groups (*APOE*−*MAPT*−, *n* = 83; *APOE*+*MAPT*−, *n* = 11; *APOE*−*MAPT*+, *n* = 34; *APOE*+*MAPT*+, *n* = 16; interaction between *APOE* and *MAPT* *P* = 0.009 in GLM). **(B)** The differences in mean cortical metrics of the regions belonging to Cluster 1 among four groups (*APOE*−*MAPT*−, *n* = 83; *APOE*+*MAPT*−, *n* = 11; *APOE*−*MAPT*+, *n* = 34; *APOE*+*MAPT*+, *n* = 16; curvature, interaction between *APOE* and *MAPT* *P* = 0.019 in GLM; folding index, interaction between *APOE* and *MAPT* *P* = 0.011 in GLM). **P* < 0.05, ***P* < 0.01, ****P* < 0.001. Error bars represent standard deviation. *APOE*−*MAPT*−, participants carrying neither *APOE* ε4 nor *MAPT* rs242557 A. *APOE*+*MAPT*−, participants carrying *APOE* ε4. *APOE*+*MAPT*−, participants carrying *MAPT* rs242557 A. *APOE*+*MAPT*+, participants carrying both *APOE* ε4 and *MAPT* rs242557 A.

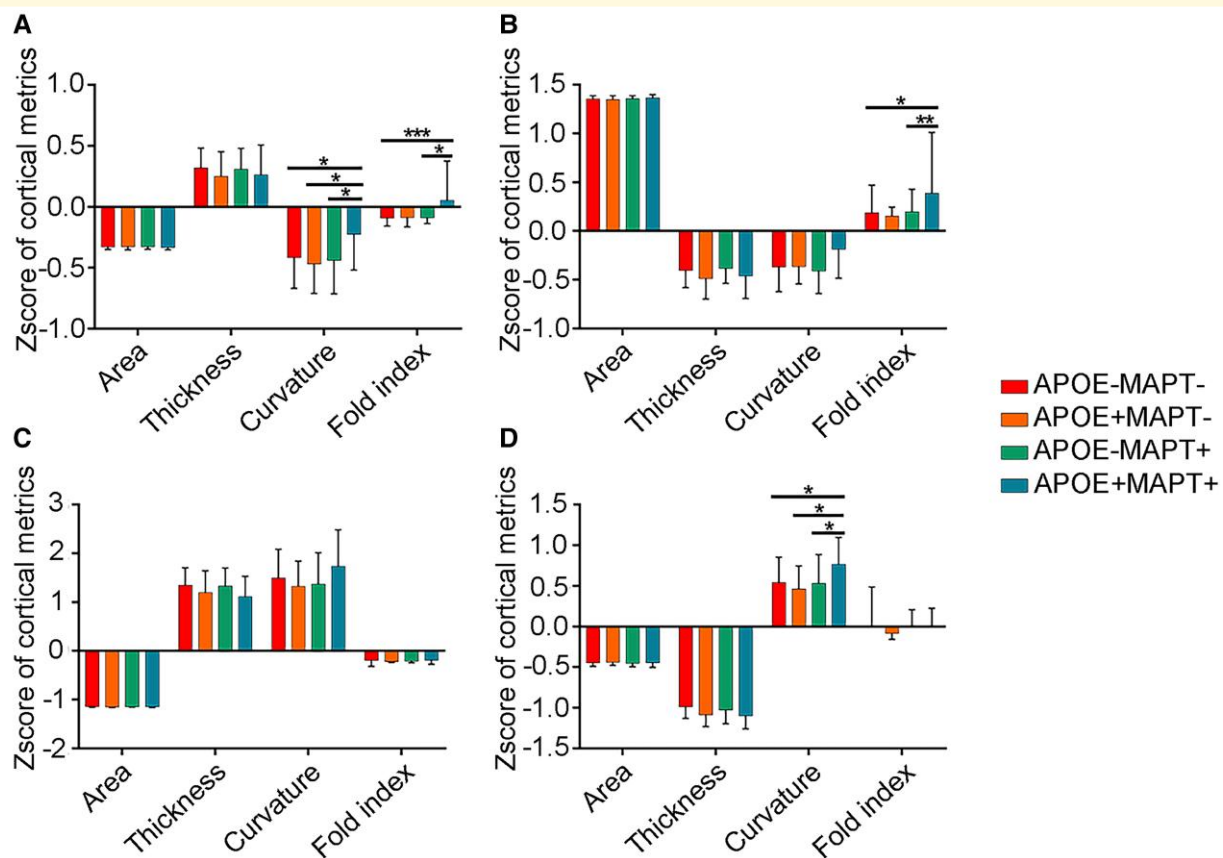


Figure 5 The interaction effect between *APOE* and *MAPT* rs242557 on mean cortical metrics of four clusters. **(A)** The differences in mean cortical metrics of the regions belonging to Cluster 1 (*APOE*−*MAPT*−, *n* = 83; *APOE*+*MAPT*−, *n* = 11; *APOE*−*MAPT*+, *n* = 34; *APOE*+*MAPT*+, *n* = 16; curvature, interaction between *APOE* and *MAPT* *P* = 0.019 in GLM; folding index, interaction between *APOE* and *MAPT* *P* = 0.011 in GLM). **(B)** The differences in mean cortical metrics of the regions belonging to Cluster 2 (*APOE*−*MAPT*−, *n* = 83; *APOE*+*MAPT*−, *n* = 11; *APOE*−*MAPT*+, *n* = 34; *APOE*+*MAPT*+, *n* = 16; folding index, interaction between *APOE* and *MAPT* *P* = 0.044 in GLM). **(C)** The differences in mean cortical metrics of the regions belonging to Cluster 3. **(D)** The differences in mean cortical metrics of the regions belonging to Cluster 4 (*APOE*−*MAPT*−, *n* = 83; *APOE*+*MAPT*−, *n* = 11; *APOE*−*MAPT*+, *n* = 34; *APOE*+*MAPT*+, *n* = 16; curvature, interaction between *APOE* and *MAPT* *P* = 0.026 in GLM). **P* < 0.05, ***P* < 0.01, ****P* < 0.001. Error bars represent standard deviation. *APOE*−*MAPT*−, participants carrying neither *APOE* ε4 nor *MAPT* rs242557 A. *APOE*+*MAPT*−, participants carrying *APOE* ε4. *APOE*−*MAPT*+, participants carrying *MAPT* rs242557 A. *APOE*+*MAPT*+, participants carrying both *APOE* ε4 and *MAPT* rs242557 A.

morphologically similar regions: (i) larger but thinner and less convoluted regions, (ii) smaller and thicker but more convoluted regions, (iii) medium sized and thicker but less convoluted regions and (iv) medium sized and thinner but more convoluted regions. The various morphological pattern might be contributed to large-scale and regionally heterogeneous development in thickness, area and convolution during adolescence and early adulthood.⁴³⁻⁴⁸ As expected, the spatial patterns identified in this study are consistent with previous studies.⁴⁹⁻⁵¹

Further analysis based on these clusters/networks revealed that the individuals carrying both *APOE* ε4 and *MAPT* A had a significant deviation from the typical morphology in the medium sized and thicker but less convoluted brain regions by increasing curvature and folding index. These regions overlapped with the regions discriminating *APOE* and *MAPT* status in the SVM analysis, such as the superior, middle and medial temporal cortex and insular and caudal

middle frontal cortex. The supervised classification and unsupervised clustering analysis gave convergent evidence supporting individuals with *APOE* ε4 and *MAPT* A tend to have higher curvature and folding index in these key brain regions. It is worth noting that these regions showed similar development and aging-related cortical thickness change and had a shared genetic influence.¹² Not only individuals with both genetic risk but also patients with schizophrenia,⁵² 22q11.2 deletions,⁵³ autistic and Asperger disorders⁵⁴ and Williams syndrome⁵⁵ showed the similar morphological characteristics, which may suggest that this kind of cortical morphology may be adverse for brain and mental health and increases vulnerability due to AD pathology in older age.

The process of forming cortical folding during brain development is complex and has not been comprehensively studied yet. However, there are several widely investigated hypotheses arguing that cortical folding is caused by the growth processes during cortical development and/or the

mechanical tension within axons.⁵⁶ Based on the axonal hypotheses, it has been speculated that synaptic pruning and reduction of connectivity during normal neurodevelopment may lead to the folding reduction from about 75th week of gestation to almost 23 years of old.⁵⁷ So, genetic risks of AD may interfere with such pruning process leading to higher folding. Recent studies have also suggested prion-like mechanisms of propagation of A β and tau proteins in AD,⁵⁸ so the individual carrying higher risk of AD may have remaining unpruned connections thus more convoluted cortex. Hyperconnectivity may promote the spread of neurodegenerative pathology when it initiates later in life. Combining with existing knowledge about the effect of *APOE* ϵ 4 and *MAPT* A on AD, these two genes may already play a significant role in shaping the brain across the lifespan by changing the cerebral structural to be more vulnerable to molecular pathology in the future.

Limitations

When considering the present study, there are several limitations. First, despite using multiple metrics to evaluate the performance of classification models, the performance of the model might be affected by the unbalance of risk groups.⁵⁹ Although statistically significant, the discriminability of models, especially the model classifying *MAPT*, was modest, so the results await future validation and replication based on larger cohorts. In addition, although our ratios of *APOE* and *MAPT* carriers are consistent with the natural frequency of these genes in non-selected population, the unbalanced groups defined by genetic risks may also impede the generalization of our conclusions to other data sets where genetic risks are enriched by including patients with dementia. Second, the cross-sectional nature of our current study makes it difficult to interpret the results and make causal inference. Although this represents a limitation of our study, it also encourages the development of more comprehensive longitudinal studies to be conducted in the healthy population for brain health related to AD in the future. Third, all the analyses in this study were based on regions of interest. Considering that the cerebrally structural variation in young adults is subtle, vertex-wised analyses may be more flexible to discover these subtle differences and unbiased by the selection of cortical parcellation. However, the high-dimensionality of imaging data and multiple comparisons problem in vertex-wised analyses introduce computational and other methodological challenges. Finally, future research is needed to consider diversity and inclusivity to cover other non-Han Chinese ethnic minorities because they have both unique and shared genetic and environmental risks for AD.

Conclusion

In summary, we discovered that AD-related risk genes *APOE* ϵ 4 and *MAPT* A have effects on the morphology of

the cerebral cortex in healthy young adults ~40–50 years before AD symptoms may occur. Our results suggest that such risks may be reflected by altered cortical morphology already detectable in healthy young adults. In addition, this study demonstrated that more attention should be paid to combine multivariate cortical features such as curvature, folding index and area in future studies and young healthy adults are at an important stage in which AD risk genes start to have an impact.

Author contributions

W.H. conducted the analyses. W.H. and L.S. drafted the manuscript. J.Z. and L.S. secured the funding and collected the data. C.R., L.S. and J.Z. co-designed the PREVENT-Dementia study. D.Z. and N.S. provided feedback on the data analysis. L.J., C.R. and J.O. provided feedback on the manuscript. L.S. provided oversight for the study.

Funding

W.H.'s participation is funded by the STI2030-Major Projects (2022ZD0213300) and China Scholarship Council. N.S.'s participation is funded by the STI2030-Major Projects (2022ZD0213300), National Natural Science Foundation of China (81471732 and 81671761), Fundamental Research Funds for the Central Universities (2017XTCX04) and Open Research Fund of the State Key Laboratory of Cognitive Neuroscience and Learning (CNLZD2101 and CNLYB2001). L.S.'s participation is funded by Alzheimer's Research UK Senior Research Fellowship (ARUK-SRF2017B-1) and NIHR Sheffield Biomedical Research Centre.

Competing interests

The authors report no competing interests.

Data availability

Anonymized data can be made available upon request if provided with aims and analysis plan. The authors will review the requests and decide whether data sharing is appropriate based on scientific rigour of the proposal and regulations on personal data protection at the time.

References

1. Jack CR Jr, Bennett DA, Blennow K, *et al.* NIA-AA research framework: Toward a biological definition of Alzheimer's disease. *Alzheimers Dement* 2018;14(4):535-562.
2. Castellano JM, Kim J, Stewart FR, *et al.* Human apoE isoforms differentially regulate brain amyloid- β peptide clearance. *Sci Transl Med.* 2011;3(89):89ra57.

3. Holtzman DM, Bales KR, Tenkova T, et al. Apolipoprotein E isoform-dependent amyloid deposition and neuritic degeneration in a mouse model of Alzheimer's disease. *Proc Natl Acad Sci U S A*. 2000;97(6):2892-2897.
4. Laws SM, Friedrich P, Diehl-Schmid J, et al. Fine mapping of the MAPT locus using quantitative trait analysis identifies possible causal variants in Alzheimer's disease. *Mol Psychiatry*. 2007;12(5):510-517.
5. Chen J, Yu JT, Wojta K, et al. Genome-wide association study identifies MAPT locus influencing human plasma tau levels. *Neurology* 2017;88(7):669-676.
6. Höglinger GU, Melhem NM, Dickson DW, et al. Identification of common variants influencing risk of the tauopathy progressive supranuclear palsy. *Nat Genet*. 2011;43(7):699-705.
7. Liu QY, Yu JT, Miao D, et al. An exploratory study on STX6, MOBP, MAPT, and EIF2AK3 and late-onset Alzheimer's disease. *Neurobiol Aging*. 2013;34(5):1519.e13-1519.e17.
8. Wang X, Huang W, Su L, et al. Neuroimaging advances regarding subjective cognitive decline in preclinical Alzheimer's disease. *Mol Neurodegeneration*. 2020;15(1):55.
9. Striepens N, Scheef L, Wind A, et al. Interaction effects of subjective memory impairment and ApoE4 genotype on episodic memory and hippocampal volume. *Psychol Med*. 2011;41(9):1997-2006.
10. Sun Y, Wang X, Wang Y, et al. Anxiety correlates with cortical surface area in subjective cognitive decline: APOE ϵ 4 carriers versus APOE ϵ 4 non-carriers. *Alzheimers Res Ther*. 2019;11(1):50.
11. Goñi J, Cervantes S, Arrondo G, Lamet I, Pastor P, Pastor MA. Selective brain gray matter atrophy associated with APOE ϵ 4 and MAPT H1 in subjects with mild cognitive impairment. *J Alzheimers Dis*. 2013;33(4):1009-1019.
12. Fjell AM, Grydeland H, Krogstad SK, et al. Development and aging of cortical thickness correspond to genetic organization patterns. *Proc Natl Acad Sci U S A*. 2015;112(50):15462-15467.
13. O'Dwyer L, Lambertson F, Matura S, et al. Reduced hippocampal volume in healthy young ApoE4 carriers: An MRI study. *PLoS One*. 2012;7(11):e48895.
14. Shaw P, Lerch JP, Pruessner JC, et al. Cortical morphology in children and adolescents with different apolipoprotein E gene polymorphisms: An observational study. *Lancet Neurol*. 2007;6(6):494-500.
15. Khan W, Giampietro V, Ginstert C, et al. No differences in hippocampal volume between carriers and non-carriers of the ApoE ϵ 4 and ϵ 2 alleles in young healthy adolescents. *J Alzheimers Dis*. 2014;40(1):37-43.
16. Scarmeas N, Stern Y. Imaging studies and APOE genotype in persons at risk for Alzheimer's disease. *Curr Psychiatry Rep*. 2006;8(1):11-17.
17. Stening E, Persson J, Eriksson E, Wahlund LO, Zetterberg H, Söderlund H. Apolipoprotein E ϵ 4 is positively related to spatial performance but unrelated to hippocampal volume in healthy young adults. *Behav Brain Res*. 2016;299:11-18.
18. Stening E, Persson J, Eriksson E, Wahlund LO, Zetterberg H, Söderlund H. Specific patterns of whole-brain structural covariance of the anterior and posterior hippocampus in young APOE ϵ 4 carriers. *Behav Brain Res*. 2017;326:256-264.
19. Cash DM, Melbourne A, Modat M, et al. Cortical folding analysis on patients with Alzheimer's disease and mild cognitive impairment. In: Ayache N, Delingette H, Golland P, Mori K, eds. *Medical image computing and computer-assisted intervention—MICCAI 2012. Lecture notes in computer science*. Springer; 2012:289-296. doi:10.1007/978-3-642-33454-2_36
20. Hu P, Qin YH, Lei FY, Pei J, Hu B, Lu L. Variable frequencies of apolipoprotein E genotypes and its effect on serum lipids in the Guangxi Zhuang and Han children. *Int J Mol Sci*. 2011;12(9):5604-5615.
21. Wang Z, Ma W, Rong Y, Liu L. The association between apolipoprotein E gene polymorphism and mild cognitive impairment among different ethnic minority groups in China. *Int J Alzheimers Dis*. 2014;2014:150628.
22. Yin R, Pan S, Wu J, Lin W, Yang D. Apolipoprotein E gene polymorphism and serum lipid levels in the Guangxi Hei Yi Zhuang and Han populations. *Exp Biol Med (Maywood)*. 2008;233(4):409-418.
23. Reuter M, Rosas HD, Fischl B. Highly accurate inverse consistent registration: A robust approach. *NeuroImage* 2010;53(4):1181-1196.
24. Segonne F, Dale AM, Busa E, et al. A hybrid approach to the skull stripping problem in MRI. *NeuroImage* 2004;22(3):1060-1075.
25. Fischl B, Salat DH, Busa E, et al. Whole brain segmentation: Automated labeling of neuroanatomical structures in the human brain. *Neuron*. 2002;33(3):341-355.
26. Fischl B, Salat DH, van der Kouwe AJW, et al. Sequence-independent segmentation of magnetic resonance images. *NeuroImage* 2004;23: S69-S84.
27. Sled JG, Zijdenbos AP, Evans AC. A nonparametric method for automatic correction of intensity nonuniformity in MRI data. *IEEE Trans Med Imaging*. 1998;17(1):87-97.
28. Fischl B, Liu A, Dale AM. Automated manifold surgery: Constructing geometrically accurate and topologically correct models of the human cerebral cortex. *IEEE Trans Med Imaging*. 2001;20(1):70-80.
29. Segonne F, Pacheco J, Fischl B. Geometrically accurate topology-correction of cortical surfaces using nonseparating loops. *IEEE Trans Med Imaging*. 2007;26(4):518-529.
30. Dale AM, Fischl B, Sereno MI. Cortical surface-based analysis: I. Segmentation and surface reconstruction. *NeuroImage* 1999;9(2):179-194.
31. Dale AM, Sereno MI. Improved localization of cortical activity by combining EEG and MEG with MRI cortical surface reconstruction: A linear approach. *J Cogn Neurosci*. 1993;5(2):162-176.
32. Fischl B, Dale AM. Measuring the thickness of the human cerebral cortex from magnetic resonance images. *Proc Natl Acad Sci USA*. 2000;97(20):11050-11055.
33. Desikan RS, Ségonne F, Fischl B, et al. An automated labeling system for subdividing the human cerebral cortex on MRI scans into gyral based regions of interest. *NeuroImage* 2006;31(3):968-980.
34. Fischl B. FreeSurfer. *NeuroImage* 2012;62(2):774-781.
35. Mourão-Miranda J, Bokde A, Born C, et al. Classifying brain states and determining the discriminating activation patterns: Support vector machine on functional MRI data. *NeuroImage* 2005;28:980-995.
36. Sato J, Fujita A, Thomaz C, et al. Evaluating SVM and MLDA in the extraction of discriminant regions for mental state prediction. *NeuroImage* 2009;46:105-114.
37. Ichimura T, Yamaguchi T. A proposal of interactive growing hierarchical SOM. In: 2011 *IEEE International Conference on Systems, Man, and Cybernetics* 2011; 3149-3154.
38. Foo H, Ng KP, Tan J, et al. Interaction between APOE- ϵ 4 and HMGB1 is associated with widespread cortical thinning in mild cognitive impairment. *J Neurol Neurosurg Psychiatry*. 2018;89(2):225-226.
39. Lu PH, Thompson PM, Leow A, et al. Apolipoprotein E genotype is associated with temporal and hippocampal atrophy rates in healthy elderly adults: A tensor-based morphometry study. *J Alzheimers Dis*. 2011;23(3):433-442.
40. Cacciaglia R, Molinuevo JL, Falcón C, et al. Effects of APOE- ϵ 4 allele load on brain morphology in a cohort of middle-aged healthy individuals with enriched genetic risk for Alzheimer's disease. *Alzheimers Dement*. 2018;14(7):902-912.
41. Fennema-Notestine C, Panizzon MS, Thompson WR, et al. Presence of ApoE ϵ 4 allele associated with thinner frontal Cortex in middle age. *J Alzheimers Dis*. 2011;26(s3):49-60.
42. Braak H, Alafuzoff I, Arzberger T, Kretschmar H, Del Tredici K. Staging of Alzheimer disease-associated neurofibrillary pathology using paraffin sections and immunocytochemistry. *Acta Neuropathol*. 2006;112(4):389-404.
43. Vijayakumar N, Allen NB, Youssef G, et al. Brain development during adolescence: A mixed-longitudinal investigation of cortical

- thickness, surface area, and volume. *Hum Brain Mapp.* 2016;37(6): 2027-2038.
44. Burgaleta M, Johnson W, Waber DP, Colom R, Karama S. Cognitive ability changes and dynamics of cortical thickness development in healthy children and adolescents. *NeuroImage* 2014;84:810-819.
 45. Lyall AE, Shi F, Geng X, *et al.* Dynamic development of regional cortical thickness and surface area in early childhood. *Cereb. Cortex.* 2015;25(8):2204-2212.
 46. Forde NJ, Ronan L, Zwiers MP, *et al.* Healthy cortical development through adolescence and early adulthood. *Brain Struct Funct.* 2017; 222(8):3653-3663.
 47. Remer J, Croteau-Chonka E, Dean DC, *et al.* Quantifying cortical development in typically developing toddlers and young children, 1–6 years of age. *NeuroImage* 2017;153:246-261.
 48. Ducharme S, Albaugh MD, Nguyen TV, *et al.* Trajectories of cortical thickness maturation in normal brain development—The importance of quality control procedures. *NeuroImage* 2016;125:267-279.
 49. Yang G, Bozek J, Han M, Gao JH. Constructing and evaluating a cortical surface atlas and analyzing cortical sex differences in young Chinese adults. *Hum Brain Mapp.* 2020;41(9):2495-2513.
 50. Chee MWL, Zheng H, Goh JOS, Park D, Sutton BP. Brain structure in young and old East Asians and Westerners: Comparisons of structural volume and cortical thickness. *J Cogn Neurosci.* 2011;23(5): 1065-1079.
 51. Sowell ER. Longitudinal mapping of cortical thickness and brain growth in normal children. *J Neurosci.* 2004;24(38):8223-8231.
 52. Schultz CC, Wagner G, Koch K, *et al.* The visual cortex in schizophrenia: Alterations of gyrification rather than cortical thickness—A combined cortical shape analysis. *Brain Struct Funct.* 2013;218(1): 51-58.
 53. Bearden CE, van Erp TGM, Dutton RA, *et al.* Alterations in midline cortical thickness and gyrification patterns mapped in children with 22q11.2 deletions. *Cereb. Cortex.* 2009;19(1):115-126.
 54. Jou RJ, Minschew NJ, Keshavan MS, Hardan AY. Cortical gyrification in autistic and asperger disorders: A preliminary magnetic resonance imaging study. *J Child Neurol.* 2010;25(12):1462-1467.
 55. Gaser C, Luders E, Thompson PM, *et al.* Increased local gyrification mapped in Williams syndrome. *NeuroImage* 2006;33(1):46-54.
 56. Zilles K, Palomero-Gallagher N, Amunts K. Development of cortical folding during evolution and ontogeny. *Trends Neurosci.* 2013;36(5):275-284.
 57. Armstrong E, Schleicher A, Omran H, Curtis M, Zilles K. The ontogeny of human gyrification. *Cereb. Cortex.* 1995;5(1):56-63.
 58. Goedert M, Clavaguera F, Tolnay M. The propagation of prion-like protein inclusions in neurodegenerative diseases. *Trends Neurosci.* 2010;33(7):317-325.
 59. Murphey YL, Guo H, Feldkamp LA. Neural learning from unbalanced data. *Appl Intell.* 2004;21(2):117-128.